

Performance comparison of yield and SMA damper on pounding vulnerability reduction for adjacent buildings under seismic loading

Kossi Jonas Sama¹⁾ and *Sourav Gur²⁾

^{1), 2)} *Department of Civil and Environmental Engineering, Indian Institute of Technology (IIT) Patna, Bihta, Patna, Bihar, India - 801103*

²⁾ sgur@iitp.ac.in

ABSTRACT

Past earthquake events showed that, even though code stipulated separation distance has been provided between adjacent building structures, mutual pounding may be observed, causing significant damage and catastrophic failure of building structures. Therefore, to mitigate such pounding induced damage, passive dampers are frequently installed between the buildings. However, due to loss of control efficiency during near fault earthquakes, conventional linear and non-linear dampers show ineffectiveness to prevent pounding. Thus, the present study explores the seismic performance of shape memory alloy (SMA) damper (SMAD) for reducing pounding vulnerability in adjacent buildings and compare with the yield damper (YD). To this end, three types of (3, 6, and 9 story) special moment resisting frames (SMRFs) are considered and modeled in SAP2000 software. Non-linear time history analysis (NLTHA) has been performed for different combination of these buildings, connected with optimally designed YD or SMAD, under 400 near fault type ground motions. Finally, the pounding vulnerability of the damper connected buildings are quantified through fragility curves, and the control efficiency of YD and SMAD have been estimated and compared. Results of the study show that, both YD and SMAD are noticeably effective in reducing the pounding. Importantly, the SMAD is highly effective, reducing up to 95 % of poundings when compared to an unconnected case, whereas YD reduces poundings almost 65 %. Further, the fragility analysis results show that, in comparison to YD, SMAD increases spectral acceleration (S_a) value on an average 80 %, for 50 % of failure probability.

Keywords: Adjacent building, pounding mitigation, yield damper, SMA damper, seismic fragility analysis, logistic regression

1. INTRODUCTION

¹⁾ Graduate Student

²⁾ Assistant Professor

Earthquakes are highly destructive natural disasters that can cause significant damage to structures and transportation systems. One particular concern is the phenomenon known as pounding, which occurs when adjacent structures collide with each other during an earthquake. This collision can lead to severe damage and even the complete collapse of building structures. Unfortunately, due to rapid urbanization and limited land availability in the big cities, structures are often constructed close to each other, without accounting the code stipulated minimum separation distance requirement to prevent pounding. Various control systems have been proposed in order to mitigate the pounding in closely spaced structure, however many of these have been proven to be inefficient and render the structure unserviceable in post-earthquake scenario. Previous study (Yaghmaei-Sabegh 2012) on pounding of adjacent building structures discovered that, the gap between two building structures has a profound impact on the maximum pounding force. Also, it has been reported that, the energy released during an earthquake can increase the pounding force as the gap distance increases. Other study (Jameel 2013) reported that, during the pounding events, taller (flexible) buildings experience higher damage than shorter (stiff) buildings. Additionally, increasing the gap distance consistently reduces story shear. In past many studies were conducted to control the seismic vibration of connect building using convention dampers as reported below.

Optimally designed nonlinear hysteretic dampers are used for vibration control of adjacent building under the random earthquake (Ni 2001). Viscoelastic and viscous dampers are being employed for vibration control of isolated and adjacent buildings, under seismic loading (Matsagar 2005 and Matsagar 2006). This control system reduces flexible building floor displacement with marginal increase in stiff building floor acceleration. Other study was conducted to control the vibration of adjacent building structures connected with the friction dampers, under harmonic base excitation and earthquake loading (Bhaskararao 2006 and Bhaskararao 2006). Further, for the connected building system, frequency domain analysis is used to study the seismic energy dissipation capacity and the vibration control efficiency of conventional viscous damper (Takewaki 2007 and Ge 2011) and nonlinear viscous dampers (Paola 2007 and Paola 2009). Maxwell dampers are utilized for controlling the seismic vibrations of the adjacent building structures (Zhang 2000 and Patel 2010), and the study results indicate presence of optimal damper design parameters and locations to minimize structural responses. Study on optimal design of viscous dampers for seismic vibration control of two connected single-degree-of-freedom (SDOF) systems shows that the mass and frequency ratio of the two systems controls the design of damper (Patel 2012). Past study estimated the seismic collapse capacity of adjacent buildings due to pounding (Kazemi 2020). In some of the recent studies (Kazemi 2021 and Kazemi 2021), linear and nonlinear fluid viscous dampers (FVDs) are used for seismic retrofitting of two adjacent buildings and predicted the collapse capacity and failure vulnerability of the buildings under pounding conditions and proposed modification factors to estimate the effects of pounding on the collapse capacities of structures.

In recent years, smart memory alloy (SMA) based control system has gained popularity in structural engineering field (DesRoches 2004 and Song 2006) dues to the

superior properties of shape memory effect (SME) and super-elasticity (SE), which is the ability to recover initial shape when subjected to stress or temperature change, and dissipate energy through flag shape hysteresis loop (Janke 2005 and Ozbulut 2011). Study on force-deformation behaviour found that SMA exhibits a broad and symmetrical hysteresis loop, making it suitable to use in the energy dissipation devices (Graesser 1991). Also, it has been observed that, both external and internal factors can influence the thermomechanical properties of SMA material, albeit with minor effects in favorable environmental conditions (Saadat 2002). Other study (Gur 2016) reported the effective application of SMAD in reducing the structures response such as floor acceleration and story drift or displacement during earthquakes, especially when the ground motion contains higher frequencies. Further, due to the shape recovery property (through SME and SE) of SMA material, SMAD installed structures shows the recentering capacity, leaving almost no or negligible residual displacement in the post-earthquake or cyclic loading scenario (Zhang 2008 and Gur 2019). Through dynamic testing it is determined that the use of SMA in frame improved its performance under applied load and ground motion (Han 2003). As reported, the energy dissipation capability of SMA wires can be enhanced by modifying the properties of the SMA material (Zhang 2007). It has been showed that, the placement and number of SMA dampers within a building can significantly reduce the seismic responses (Qian 2013).

Thus, due to SE and SME properties, SMAD have an edge over other dampers. Most of the research works focuses on the seismic vibration control and retrofitting of single building. Study of SMAD for seismic vibration control of adjacent and connected building structures is very scant. Some of the very recent studies focus on the control efficiency of SMAD for adjacent linear and nonlinear buildings under the seismic loading (Gur 2020, Singh 2022 and Patel 2022). In a parametric study on the seismic performance assessment of SMAD connected buildings reported that, an appropriate choice of the SMAD parameters can substantially reduce the peak floor acceleration, peak floor displacement, and residual displacement than that of the YD connected buildings (Gur 2022). Optimal design of YD and SMAD for connected building under stochastic earthquake is reported in a very recent study (Sama 2023) and showed superior optimal response control efficiency of SMAD over YD. Thus, numerous studies have examined the response reduction capacity of SMAD and some of them focuses on response reduction for connected buildings. But none of them address the potential of SMAD to reduce the pounding vulnerability under seismic loading, where this study stands out as unique. Further, the pounding vulnerability reduction efficiency of SMAD is compared with YD. To this end, different SMRF buildings connected with YD or SMAD are considered. Nonlinear time history analysis (NLTHA) are performed under 400 recorded ground motions. Finally, using the results of NLTHA, pounding vulnerability is estimated and compared for YD or SMAD connected buildings, through fragility curves.

2. MODELING OF BUILDING

In this study, 3, 6, and 9 story SMRF buildings are modeled in SAP2000 software. It is assumed that buildings are either unconnected or connected through YD and superelastic SMAD. Design of the buildings as shown in Fig. 1 (with all dimensions are

in meters (m)) was intended for a specific location with coordinates of 37.88° N latitude and 122.08° W longitude, as well as soil classification D. The seismic design criteria adopted were $SD_1 = 0.6 \text{ g}$ and $SD_5 = 1.25 \text{ g}$. Here, the response modification factor (R) value of 8, deflection amplification factor (C_d) value of 5.5, and system over-strength factor (X) value of 3 are utilized. As per the previous study, the dead and live loads for the roof are considered as 1.68 kN/m^2 and 0.96 kN/m^2 , respectively; while for the other floors, they are taken as 3.35 kN/m^2 and 1.68 kN/m^2 (Kitayama 2016). In the building frame, material nonlinearity is incorporated through lumped plasticity approach. Based on the table 5-6 in FEMA-356, nonlinear behaviour of column hinges are defined through axial force-bending moment (PM3) interaction property, and flexural hinges (M3) are provided for beam. Hinges are provided at both the ends of a member, 0.05L (i.e. 5 % of member length) distance away from the support or beam-column joint. Using the modal analysis result from SAP2000 fundamental time periods are estimated as 0.54 s, 0.97 s, and 1.41 s for 3, 6, and 9 story SMRF building frames.

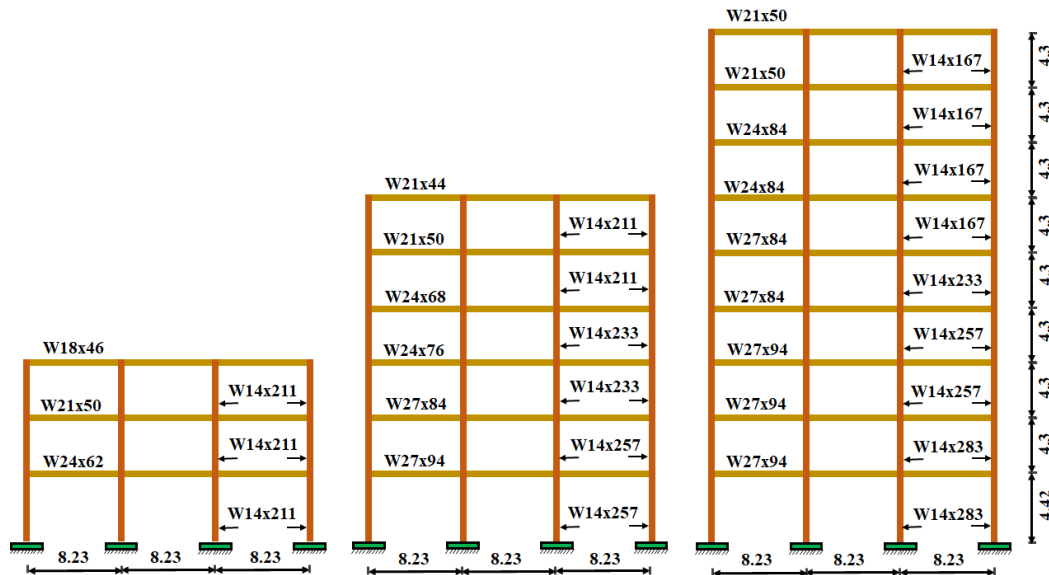


Fig. 1 Elevation and section arrangement of the 3, 6, and 9 story SMRF buildings

One crucial element of an all-encompassing seismic design is to consider the minimum separation distance between two adjacent buildings. Besides, other aspects such as the structural design of the building, the conditions of the site, and potential seismic dangers such as liquefaction should also be considered. During an earthquake, it is essential to maintain a safe distance between neighboring structures to prevent mutual pounding. This separation distance is crucial to ensure that the buildings don't collide and lead to significant damage or even collapse. The American Society of Civil Engineers (ASCE) has provided guidelines for determining the minimum separation distance between closely placed buildings. ASCE/SEI 7-10, section 12.12.3 indicates that several factors such as the deflection amplification factor (C_d), the maximum elastic displacement (δ_{max}) and the importance factor (I) determine the minimum separation distance, as given by Eq. (1)

$$\Delta_{MT} = \sqrt{\left(\frac{C_d \cdot \delta_{max}}{I}\right)_1^2 + \left(\frac{C_d \cdot \delta_{max}}{I}\right)_2^2} \quad (1)$$

The deflection amplification factor, which is defined in Table 12-2-1 of ASCE/SEI 7-10, quantifies the degree to which a building will deflect when subjected to seismic loads. The importance factor assesses the significance of the building to society and the economy. The maximum distance that a structure can move during an earthquake before it starts to deform inelastically is known as the maximum elastic displacement (δ_{max}). For each case of these three buildings, a push over analysis is carried out to determine the maximum elastic displacement (δ_{max}). From the push over analysis results (as shown in Fig. 2), the maximum elastic displacement (δ_{max}) is determined as 0.15 m, 0.28 m and 0.37 m for 3, 6, and 9 story SMRF building structures, respectively.

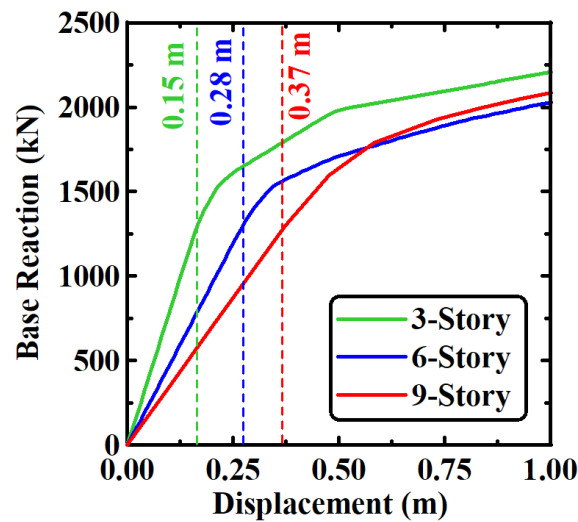


Fig. 2 Push over analysis curve for 3, 6, and 9 story SMRFs building structures

3. MODELING OF DAMPER

In this study, two different types of dampers, namely, yield damper (YD) and SMA dampers (SMAD) are used to suppress the seismic vibration of connected buildings. Dampers are connected between each floor of the flexible (tall) building and stiff (short) building. The dampers are mainly composed of steel or SMA springs, cylinder and piston assembly, and rigid steel link, as shown in the schematic diagram in Fig. 3. In previous studies (Gur 2019, Gur 2020, Singh 2022 and Gur 2022), Bouc-Wen material model is used to numerically model the force displacement hysteresis loop of the YD. For SMAD, to capture the hysteresis behaviour of SMA, different material model such as Graesser-Cozzarelli's (Graesser 1991) and Yan and Nie (Yan 2000) are used in previous studies (Gur 2016, Gur 2019, Gur 2020, Singh 2022, Gur 2022 and Sama 2023). Here, to capture the nonlinear force-displacement hysteretic behaviour, YD and SMAD are model using Wen plastic link element and multi-linear elastic and plastic link element, respectively. As

stated, for each different combinations of the structures the dampers are connected at each floor level between the structures with appropriate damper strength, as obtained from the previous optimization study (Sama 2023). More detail about the YD and SMAD modelling is provided below.

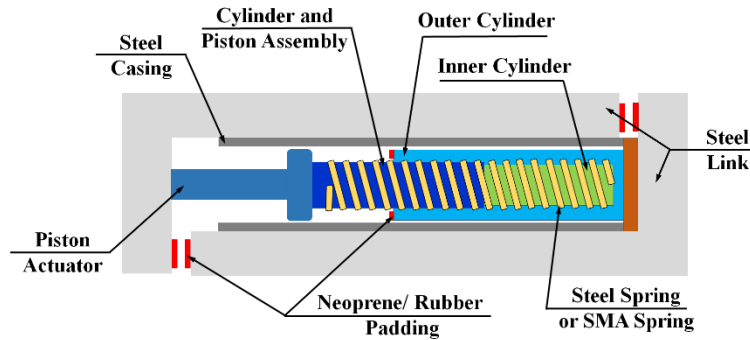


Fig. 3 Schematic view of yield damper (YD) or superelastic SMA damper (SMAD)

3.1 Model of yield damper (YD)

To simulate the hysteresis behaviour of YD, a wen plasticity link element is used, as available in SAP2000. This model is designed to replicate the nonlinear force displacement behavior of metallic materials by focusing on the plastic deformation, which occurs when a material is subjected to stress that exceeds its elastic limit. The nonlinear force displacement relation of wen plastic model is given by

$$F = \alpha_y k_y u + (1 - \alpha_y) F_y z \quad (2)$$

$$\dot{z} = \left(\frac{k_y}{F_y} \right) \begin{cases} \dot{u}(1 - |z|^\eta) & \text{if } \dot{u}z > 0 \\ \dot{u} & \text{otherwise} \end{cases} \quad (3)$$

where k_y is elastic stiffness of damper, α_y is the ratio of post-yield to elastic stiffness, F_y indicate the yield strength of damper, u and \dot{u} are the displacement and velocity, respectively. Here, z is the nondimensional parameter represent hysteresis behaviour.

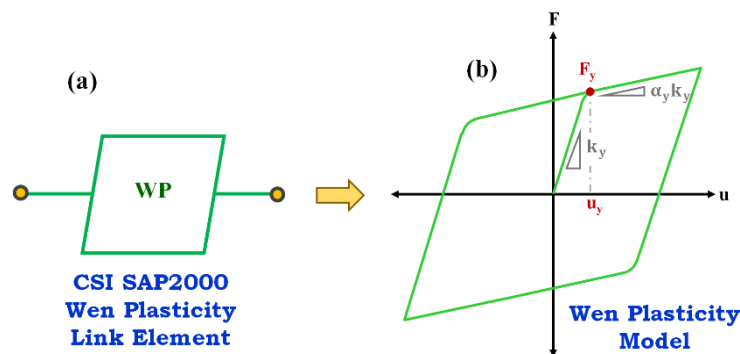


Fig. 4 Model of yield damper (YD) (a) wen plastic link element and (b) hysteresis loop

The initial value of z is 0 with the range $|z| \leq 1$. The parameter η control the shape and transition (elastic to plastic) of the hysteresis loop. It is to note that, with increase in the value of η , the bilinear transition becomes sharp. The above parameters are the critical inputs for modeling YD in SAP2000, and to generate the desire force-deformation characteristic. Fig. 4 (a) shows the arrangement of the link element which can capture the hysteresis behaviour of the YD as shown in Fig. 4 (b).

3.2 Model of SMA damper (SMAD)

Two important properties of SMA material are shape memory effect (SME) and superelasticity (SE). SME is a property of SMA material to recover its original shape by heating due to the microstructure reorientation, whereas SE feature makes the SMA to come back to its original position when unloaded, and shows the flag shaped hysteresis loop as reported in previous study (Dolce 2000). This specific feature has a lot more civil engineering application as reported in previous studies (Song 2006 and Ozbulut 2011). SMA is available in different shape such as, wires, spring, bars, and rings etc. However, Nitinol (NiTi) spring is used in this study and properties are taken from other study (Qiu 2020), as provided in Table 1. Here in Table 1, E_A and E_M refers to the Young's modulus of the austenite and martensite phase of SMA, σ_{AM}^s and σ_{AM}^f are the austenite to martensite phase transformation start and finish stress, σ_{MA}^s and σ_{MA}^f are the martensite to austenite phase transformation start and finish stress, and ϵ_r is the maximum recovery strain due to phase transformation.

Table 1: Material properties of SMA stress strain loop (Qiu 2020)

E_A	E_M	σ_{AM}^s	σ_{AM}^f	σ_{MA}^s	σ_{MA}^f	ϵ_r
22 GPa	20GPa	340 MPa	650 MPa	500 MPa	150 MPa	0.035

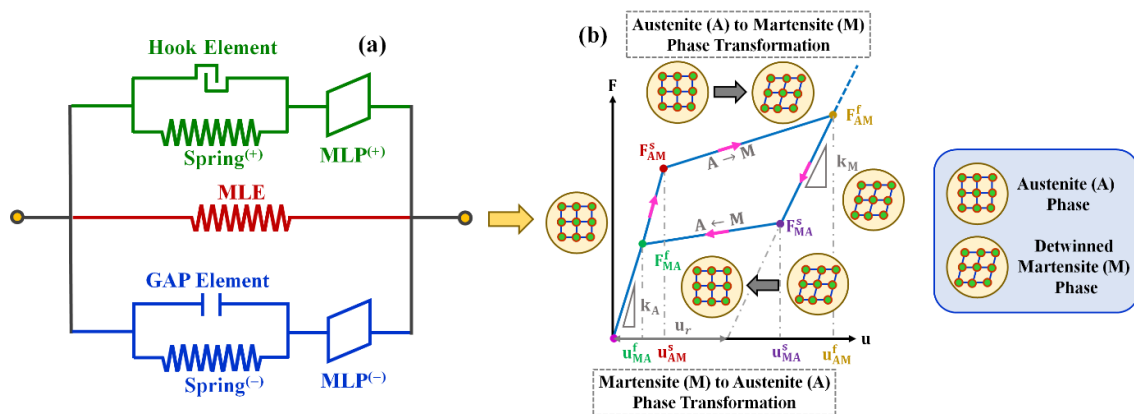


Fig. 4 Model of SMA damper (SMAD) (a) arrangement different link elements and (b) force displacement hysteresis loop of SMA

Previously, to simulate the flag shaped hysteresis loop of SMA, CSI SAP2000 proposed knowledgebase model based on the multi linear elastic (MLE) and multi linear plastic (MLP) link element. The disadvantage of this SMA model is in the cumulative damage action of MLP link element. Thus, to overcome this limitation, a recent study

(Domenico 2021) have suggested a different modeling technique for the SMA damper, which is both more intricate and adaptable. The new model includes not only the MLE link element, but also gap and hook link elements, as well as two MLP link elements (one in tension phase and other compression phase i.e. MLP positive and MLP negative). The addition of gap and hook link elements prevents the degradation MLP negative and MLP positive link elements under multi-cycle compression and tension loading. Here, force and displacements are the basic input for the link elements. The MLP link property exhibits the hysteresis behaviour under cyclic loading. To simulate this, among several available hysteresis model, the pivot model is chosen which can capture the flag shaped loop as well as the recentering behaviour of SMA. For this, value of different parameters of the pivot model are taken as $\alpha_1 = \alpha_2 = \infty$, $\beta_1 = \beta_2 = 0$, and $\eta = 1$. Fig. 5 (a) represents the proposed model in SAP2000 (using different link elements) and Fig. 5 (b) shows a typical force displacement loop of SMA damper. The MLE link provides nonlinear but elastic behaviour having an initial slope of k_E . It is considered that the MLE link property traverse the lower limb of the force deformation curve of SMA. To estimate the critical force and displacement values in Fig. 5 (b), Table 1 parameters along with the SMA spring size and length has been used. The accuracy of proposed model is validated from the experimental hysteresis loop behavior of the previous study (Qiu 2020), and it shows very good agreement.

3.3 Force displacement hysteresis loop

This section discusses the force displacement hysteresis behavior YD and SMAD when subjected to multiple cycle displacement. For this, the dampers were tested by subjecting two-cycle triangular displacement excitation, as illustrated in Fig. 6 (a). Force displacement hysteresis loop of YD and SMAD under given cyclic loading is shown in Fig. 6 (b) and (c), respectively. Here, the wen plastic link element and newly proposed SMA link element can sufficiently capture the hysteresis behaviour of YD and flag shape hysteresis of SMAD under cyclic loading. Further from Fig. 6 (b) and (c) it is clear that, area under SMAD force displacement hysteresis loop is slightly less than YD; and thus, SMAD provide little less energy dissipation capacity than YD. However, at the end of displacement cycle, SMAD offers much better recentering ability than the YD, i.e. SMAD leaves almost no residual displacement at zero force level, whereas YD shows large residual displacement.

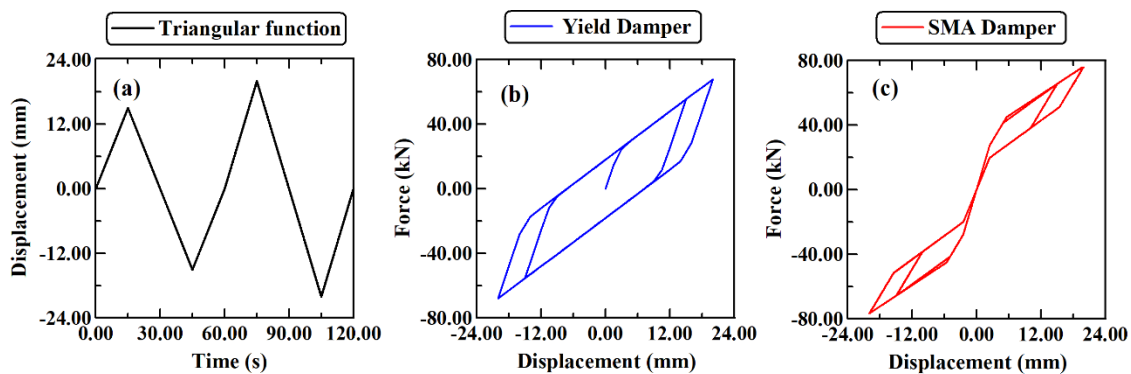


Fig. 6 Hysteresis loop of Yield and SMA and Yield damper under cyclic loading

4. GROUND MOTION SCALING

The process of scaling ground motions is important for earthquake engineering that involves adjusting recorded data to correspond the anticipated ground motion at a specific location. It is necessary to ensure that structures are designed to withstand the ground motion experienced during an earthquake, as the severity of the ground motion can have a significant impact on the structure's behavior, integrity and serviceability for ensuring the safety of the occupants and minimizing damage. In this study, 400 ground motions were used and their acceleration spectrum was adjusted to match the design response spectrum for the site's soil type, risk category, and seismic design parameters, with $SD_1 = 0.6 \text{ g}$ and $SD_5 = 1.25 \text{ g}$. The ASCE 7 hazard tool is utilized to obtain the design response spectra. The scaling process involves determining the equivalent expected ground motion at the site of interest through multiplying the recorded ground motion data by a scaling factor, which was calculated using Eq. (4)

$$SF = \frac{\sum(S_{a_{GM}} * S_{a_{ASCE}})}{\sum(S_{a_{GM}})^2} \quad (4)$$

Here $S_{a_{GM}}$ and $S_{a_{ASCE}}$ are the spectral acceleration (S_a) for individual ground motion and the design response spectra from ASCE 7-10. The S_a corresponding to each ground motion is compared to the design response spectra from the ASCE 7-10 code, using above stated process, and matched within a 10% tolerance limit for a range of 0.2 times the stiff building time period to 1.5 times the flexible building time period. To perform this task and for NLTHA, the time step of individual ground motion is set at 0.001 s. Fig. 7 (a) shows the S_a of individual ground motion and average S_a . Fig. 7 (b) provides the comparison of the average S_a with the ASCE 7-10 design response spectra, and it shows a significant difference between them. Fig. 7 (c) shows that, after performing the spectral matching, average S_a of scaled ground motions matches very well (within tolerance limit and time period) with design response spectra of ASCE 7-10.

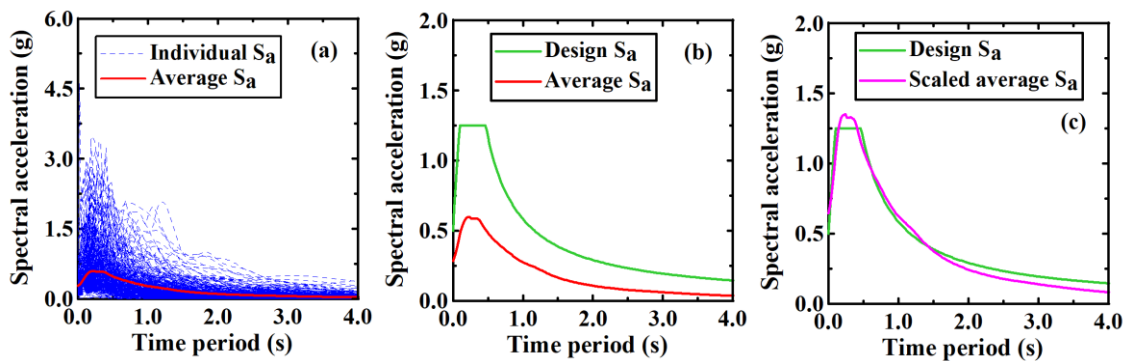


Fig. 7 Variation of different spectral acceleration with time period

5. POUNDING VULNERABILITY ASSESSMENT

Assessment of the pounding vulnerability for flexible and stiff buildings include the calculation of damage condition, considering whether there was pounding or not, for every ground motion. This is established by comparing the difference in displacement

between the floors of flexible and stiff buildings at any given time instant (accounting the separation distance between them), as given in Eq. (5)

$$\Delta = \text{separation distance} + (\delta_{sb} - \delta_{fb}) \quad (5)$$

In this context, δ_{sb} and δ_{fb} represents the displacement at a specific floor level in stiff and flexible building. The presence of pounding is determined by whether or not $\Delta \geq 0$; if it is greater than zero then there is no pounding i.e. pounding state is 0, and if it is not, then pounding state is equal to 1. If any floor level in the flexible or stiff building experiences pounding, then it is marked for that corresponding S_a value of the ground motion, resulting in a binary distribution of pounding or no pounding i.e. '1' or '0'. Additionally, if multiple levels in the flexible or stiff building experience pounding during the ground motion, then the total number of affected floor levels is calculated and plotted against the corresponding S_a value of that particular ground motion. It is important to note that the number of levels affected cannot exceed the total number of floors in the stiff building. Using this analysis, a distribution was generated that shows the total number of affected floors for each combination of buildings in relation to the S_a . Also, the present study provides additional information by assuming the existence of three levels of damage states where DS_1 representing one third of the total number of stiff building floors pounded, DS_2 representing two thirds of the total number of stiff building floors pounded, and DS_3 representing more than two thirds or all of the total number of stiff building floors pounded. After defining the damage states, fragility analysis is performed to determine the pounding vulnerability (probability) through fragility curve method. The pounding data is used to develop the fragility curves, as discussed subsequently.

5.1 Analytical fragility curve model

In this method of fragility analysis, median and log-standard deviation of fragility curves for the different damage states are estimated simultaneously with the aid of maximum likelihood method (Shinozuka 2000 and Shinozuka 2000) where a single log-standard deviation is assumed for all damage state. Due to the use of a constant log standard deviation for different damage states, fragility curves for different damage states do not cross each other. The fragility curves associated with these scenarios indicate the likelihood, denoted by the probability $P_{ik} = P(a_i, DS_k)$, that a particular ground motion with a certain spectral acceleration value ($S_{a_i} = a_i$) will produce a specific damage state (DS_k). Thus, if pounding between flexible and stiff buildings is assisted with respect to a certain spectral acceleration value ($S_{a_i} = a_i$), then the pounding probability at a particular damage state (DS_k) is expressed as:

$$F_k(a_i; c_k, \zeta) = \Phi \left[\frac{\ln(a_i/c_k)}{\zeta} \right] \quad (6)$$

Here, the fragility curves for "1/3", "2/3" and "all floors" pounding is denoted by $k = 1, 2, \text{ and } 3$, respectively; and can be characterized by their median c_k and log standard deviation ζ . For different damage state pounding probability is denoted as

$$P_{i1} = P(a_i, D_1) = 1 - F_1(a_i; c_1, \zeta) \quad (7)$$

$$P_{i2} = P(a_i, D_2) = F_1(a_i; c_1, \zeta) - F_2(a_i; c_2, \zeta) \quad (8)$$

$$P_{i3} = P(a_i, D_3) = F_2(a_i; c_2, \zeta) - F_3(a_i; c_3, \zeta) \quad (9)$$

$$P_{i4} = P(a_i, E_4) = F_3(a_i; c_3, \zeta) \quad (10)$$

The likelihood function can then be computed as

$$L(c_1, c_2, c_3, \zeta) = \prod_{i=1}^n \prod_{k=1}^4 P_k(a_i, DS_k)^{\eta_{ik}} \quad (11)$$

where, $\eta_{ik} = 1$ is the damage state DS_k occurs for the i^{th} ground motion of $S_{a_i} = a_i$ and $\eta_{ik} = 0$ otherwise. Maximum likelihood method is used in the following way to calculate different medians for different damage states (c_1, c_2, c_3) and a common log-standard deviation (ζ) for all the damage states.

$$\frac{\partial \ln L(c_1, c_2, c_3, \zeta)}{\partial c_k} = \frac{\partial \ln L(c_1, c_2, c_3, \zeta)}{\partial \zeta} = 0 \quad (\text{for } k = 1, 2, 3) \quad (12)$$

5.2 Machine learning (ML) method for fragility curve prediction

The objective of this section is to create a ML based curve-fitting model that can map the spectral acceleration (i.e. S_a , as the primary input parameter), to the probability of pounding or no pounding, represented as a binary output. To accomplish this, logistic regression model is employed, which utilizes the sigmoid function to predict probability between 0 and 1 for any input. The sigmoid function is given by

$$g(z) = \frac{1}{1 + e^{-z}} \quad (13)$$

To apply this function, at first the input for the sigmoid function has been computed as a linear regression output to the log normal of the $S_{a_i} = a_i$, as given by

$$z = f_{w,\theta}(z) = w * \ln(a_i) + \theta \quad (14)$$

Here, w and θ are the parameters that constitute the logistic regression model. These parameters will be optimized for the best fit of the model by minimizing the cost function through the gradient descent method. For this the results of 400 NLTHA are used for the corresponding values of spectral acceleration $S_{a_i} = a_i$. The pounding probability between 0 and 1 is compute the using the sigmoid function as:

$$P_{exp} = g(w * \ln(a_i) + \theta) = \frac{1}{1 + e^{-[w * \ln(a_i) + \theta]}} \quad (15)$$

6. RESULT AND DISCUSSION

At first using the NLTHA results, a distribution was generated that shows the total number of affected floors for each combination of buildings (6F-3S, 9F-3S, and 9F-6S) in relation to the S_a as illustrated in the Fig. 8. Here, the 'F' and 'S' denotes flexible and stiff building, respectively. Note that, during an earthquake event, the maximum number of floors can pound is same as the total number of floors in stiff building. Fig. 8 (a1) to (c1) shows the pounding results of 6F-3S building combination, without damper, and connected with YD or SMAD. Absence of YD or SMAD shows significant level of

pounding which could harm up to two floors out of the three floors, and pounding of a single floor or double floors are equally observed. But, the presence of YD led to the mitigation of most of the ground motion causing double floor pounding, and shows only one floor experiencing pounding or no pounding. Analysis of pounding or no pounding showed that YD decreased damage by 66%. Compare to YD, SMAD performed even better, and reduce the pounding to only one floor, particularly at the higher values of S_a . Thus, SMAD reduced pounding events by 96% and 88%, when compared with the unconnected and the YD connected 6F-3S building; respectively. Fig. 8 (a2) to (c2) depicts the pounding events for 9F-3S building, at unconnected condition and at YD or SMAD connected case. It can be observed for the unconnected building that, the pounding occurs maximum up to two floors out of the three floors, predominantly affecting only one floor. Presence of the YD or SMAD either completely mitigates or reduced to single floor pounding. It has been observed that, YD or SMAD reduces the severity of pounding damage by 92% than unconnected building.

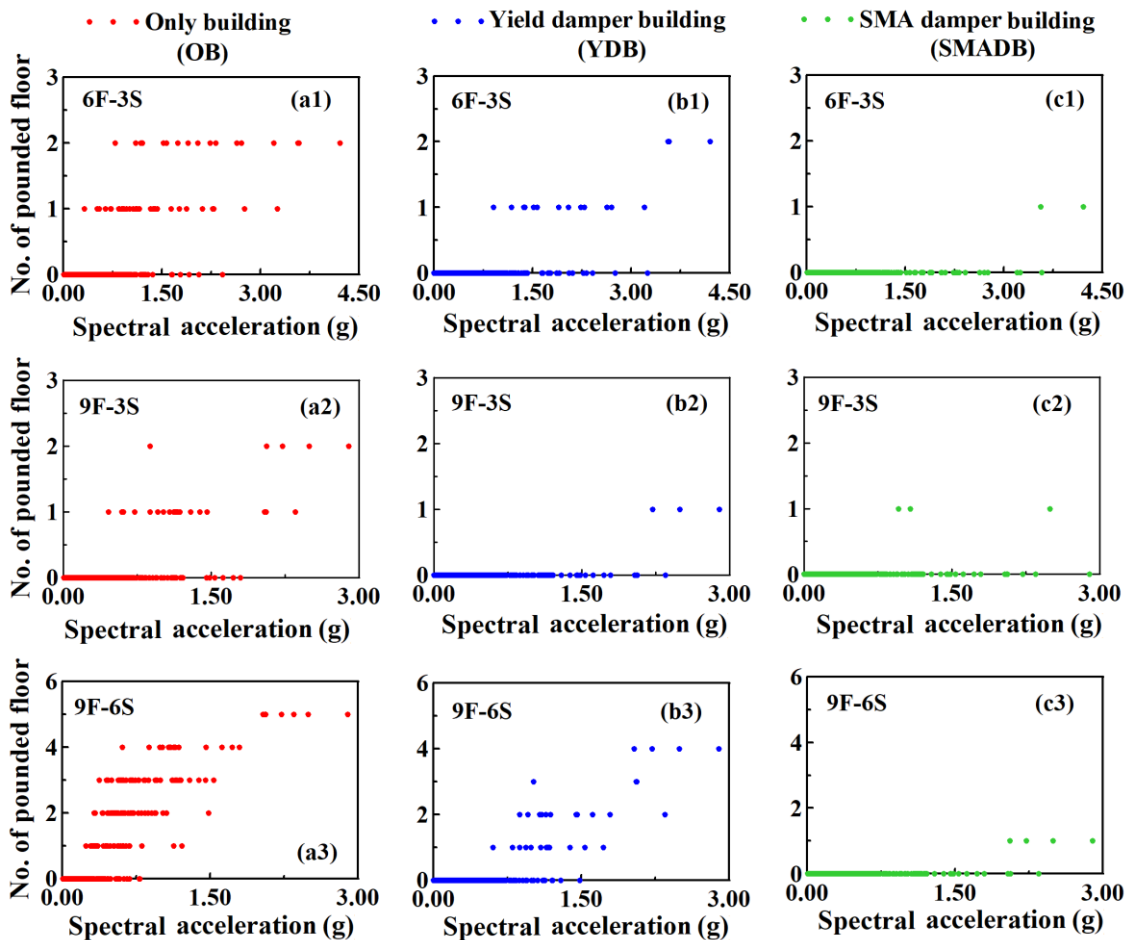


Fig. 8 Distribution of the number of pounded floors with respect to the spectral acceleration for (a1)-(c1) 6F-3S, (a2)-(c2) 9F-3S, and (a3)-(c3) 9F-6S unconnected building (i.e. only building), YD, and SMAD connected buildings

Finally, the results of 9F-6S unconnected, YD, and SMAD connected buildings cases are shown in Fig. 8 (a3) to (c3), and it reveals that, significant pounding occurs in the absence of YD or SMAD. For unconnected building (i.e. only building), the pounding affects uniformly up to five floors out of the six floors, and is more severe with higher S_a level. However, the installation of YD resulted in a reduction of the maximum number of pounded floors (up to four) and changes the distribution of pounded floors with respect to the S_a . Presence of YD either reduces the number of pounded floors or causing no pounding, and it thereby mitigates 76% of pounding than unconnected buildings. Extraordinary performance is observed in the case of the SMAD connected 6S-9F buildings, which reduced the maximum number of pounded floors to only one floor. As found, SMAD reduced pounding by 96% compared to unconnected building and 84% compared to YD connected building.

Next, using the above data pounding vulnerability of the buildings are assess and the fragility curves has been drawn. Initially, the fragility curves have been drawn to demonstrate the likelihood of pounding or no pounding in each of the three scenarios. The Fig. 9 (a)-(c) illustrates the probability of pounding for 6F-3S, 9F-3S, and 9F-6S building combinations, with respect to S_a . For all cases, with increasing S_a probability of pounding increases. The slope of the fragility curve indicates the structure's sensitivity on S_a against pounding. It can be observed that, the fragility curves of the 9F-6S building (Fig. 9 (c)) and the SMAD connected 6F-3S building (Fig. 9 (a)) exhibit a steep slope due to the high likelihood of pounding beyond a certain level of S_a . On other hand, in Fig. 9 (a) 6F-3S unconnected building and YD connected building, and in Fig. 9 (b) all 9F-3S buildings display flatter slopes, implying the buildings are more resilient, and can tolerate larger increases in S_a value, maintaining an acceptable level of pounding. This observation can be explained using Fig. 8, where the original data for unconnected or only building and the YD connected building show significant pounding occurrences, while the buildings with SMAD have fewer pounding occurrences, resulting in a little overlap in the non-pounding and pounding S_a data. This lack in overlap leads to a small standard deviation, and a certain shift from no pounding to pounding, beyond a specific value of S_a . Conversely, if there is considerable overlap in the S_a data of non-pounding and pounding, the likelihood of pounding is less certain, resulting in a flatter fragility curve with less sensitive to S_a value variation. Different parameters fragility curves (median and log standard deviation of S_a) are provided in Table 2, for different combination of buildings. It can be observed that, the median vale of S_a (i.e. 50 % probability) increases noticeably in presence of damper, specifically for SMAD than YD. Compare to unconnected building (i.e. OB), YD connected building (i.e. YDB) increases median vale of S_a by 66% for 6F-3S, 99% for 9F-3S, and 140% for 9F-6S combination of buildings. Whereas, for SMAD connected building (i.e. SMADB) this improvement becomes (compare to the OB) by 146% for 6F-3S, 266% for 9F-3S, and 389% for 9F-6S combination of buildings. Therefore, compare to YD, SMAD enhances median vale of S_a by 48% for 6F-3S, 84% for 9F-3S, and 104% for 9F-6S combination of buildings. Further, in contrast to the OB, presence of damper reduces the uncertainty in prediction of pounding possibility (probability) via decreasing log standard deviation value. YD connected building reduces the log standard deviation value of S_a by 15%, 6%, and 24% for 6F-3S, 9F-3S, and 9F-6S combination of buildings, respectively, when compare with

the OB. Similarly, for the SMAD connected building this reduction become 60%, 44%, and 63% for the 6F-3S, 9F-3S, and 9F-6S combination of buildings, respectively. Thus, compare to YD, SMAD reduces the log standard deviation value of S_a by 53%, 41%, and 52% for 6F-3S, 9F-3S, and 9F-6S combination of buildings, respectively. Therefore, it can be stated that, SMAD not only enhances the capacity (in terms of the S_a) of buildings to resist pounding, also reduces the uncertainty in predicting prediction, in contrast to the unconnected or YD connected buildings.

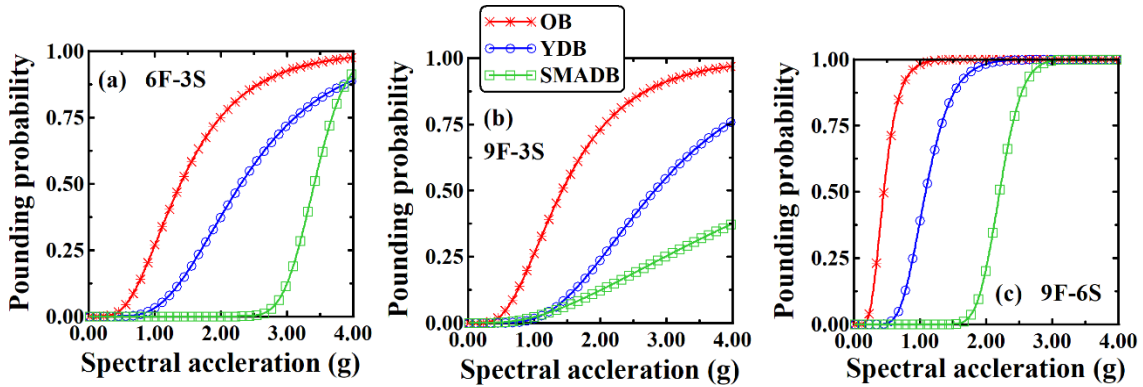


Fig. 9 Fragility curve of pounding probability with respect to spectral acceleration for (a) 6F-3S (b) 9F-3S, and (c) 9F-6S buildings connected without and with dampers

Table 2: Values of spectral acceleration for overall pounding fragility

Building combination	Median (c)			Log standard deviation (ζ)		
	OB	YDB	SMADB	OB	YDB	SMADB
6F-3S	1.39	2.30	3.41	0.53	0.45	0.21
9F-3S	1.42	2.82	5.20	0.52	0.49	0.29
9F-6S	0.45	1.09	2.20	0.38	0.29	0.14

Table 3: Values of spectral acceleration for different damage state pounding fragility

Building combination	Median (c)			Log standard deviation (ζ)		
	OB	YDB	SMADB	OB	YDB	SMADB
Damage state 1 (DS_1) indicating 1/3 floor pounding						
6F-3S	1.38	2.20	3.41	0.53	0.45	0.21
9F-3S	1.35	2.82	5.20	0.52	0.49	0.29
9F-6S	0.45	1.09	2.20	0.38	0.29	0.14
Damage state 2 (DS_2) indicating 2/3 floor pounding						
6F-3S	2.36	4.18	-	0.53	0.45	-
9F-3S	2.98	-	-	0.52	-	-
9F-6S	0.81	1.96	-	0.38	0.29	-
Damage state 3 (DS_3) indicating all floor pounding						
6F-3S	-	-	-	-	-	-
9F-3S	-	-	-	-	-	-

9F-6S	2.16	-	-	0.38	-	-
-------	------	---	---	------	---	---

The fragility curves under individual damage state for different cases of buildings without and with damper are shown in Fig. 10. 1/3 and 2/3 floor pounding probability for 6F-3S building case without and with YD and SMAD is shown in Fig. 10 (a1) and (b1). Similarly, for the 9F-3S building without and with YD and SMAD, the 1/3 and 2/3 floor pounding probability is shown in Fig. 10 (a2) and (b2). Note that, for 6F-3S and 9F-3S buildings, none of the cases show all floor pounding condition, and importantly SMAD limits the damage state only to the 1/3 floor pounding case. Fig. 10 (a3) to (c3) depicts the pounding probability for different damage state of 9F-6S building case without and with YD and SMAD. Here SMAD limits the pounding to only 1/3 floor, which is absent for YD connected building, and pounding observed till 2/3 floor case. This proves the superior control efficiency of the SMAD over YD, even for reducing the individual damage state. Table 3 provides the different statistical parameters (median and log standard deviation of S_a) of pounding for all three damage states. As before, in contrast to the unconnected and YD connected buildings, SMAD connected building shows substantial increases in median values of S_a and decrease in log standard deviation values of S_a , for different pounding damage state of all building cases.

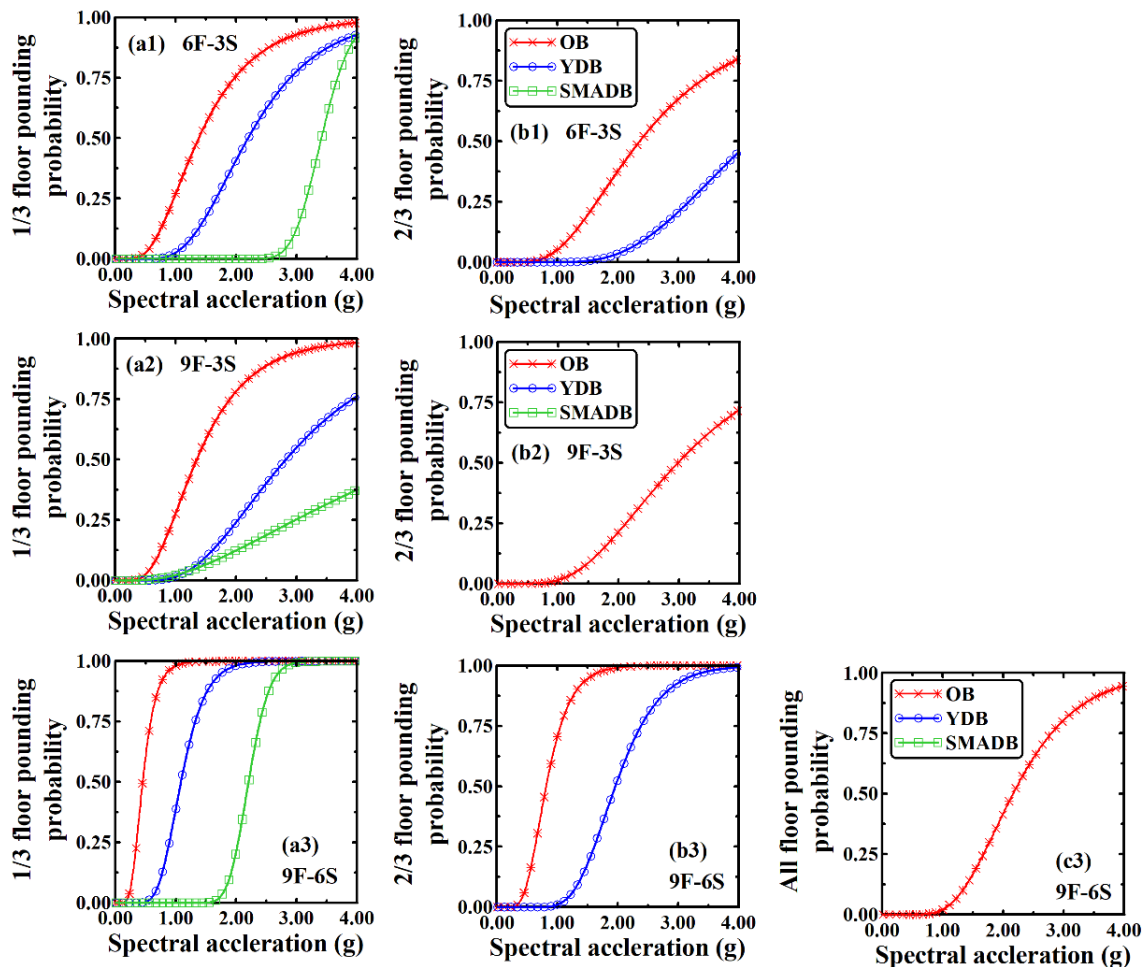


Fig. 10 Fragility curve of different damage state for pounding probability with respect to spectral acceleration for (a1)-(b1) 6F-3S (a2)-(b2) 9F-3S, and (a3)-(c3) 9F-6S buildings

To predict the overall pounding probability with respect to S_a , the machine learning (ML) regression-based fragility curves are plotted in Fig. 11, and compared with the analytical fragility curves. Here, logistic regression method is used to develop the ML based fragility curves. Fig. 11 (a1) to (c1) and Fig. 11 (a2) to (c2) shows the ML based and analytical fragility curves for 6F-3S and 9F-3S building cases, respectively, without and with YD and SMAD. It can be found, maximum difference between ML and analytical fragility curves are below 5%, which proves the robustness of the ML method.

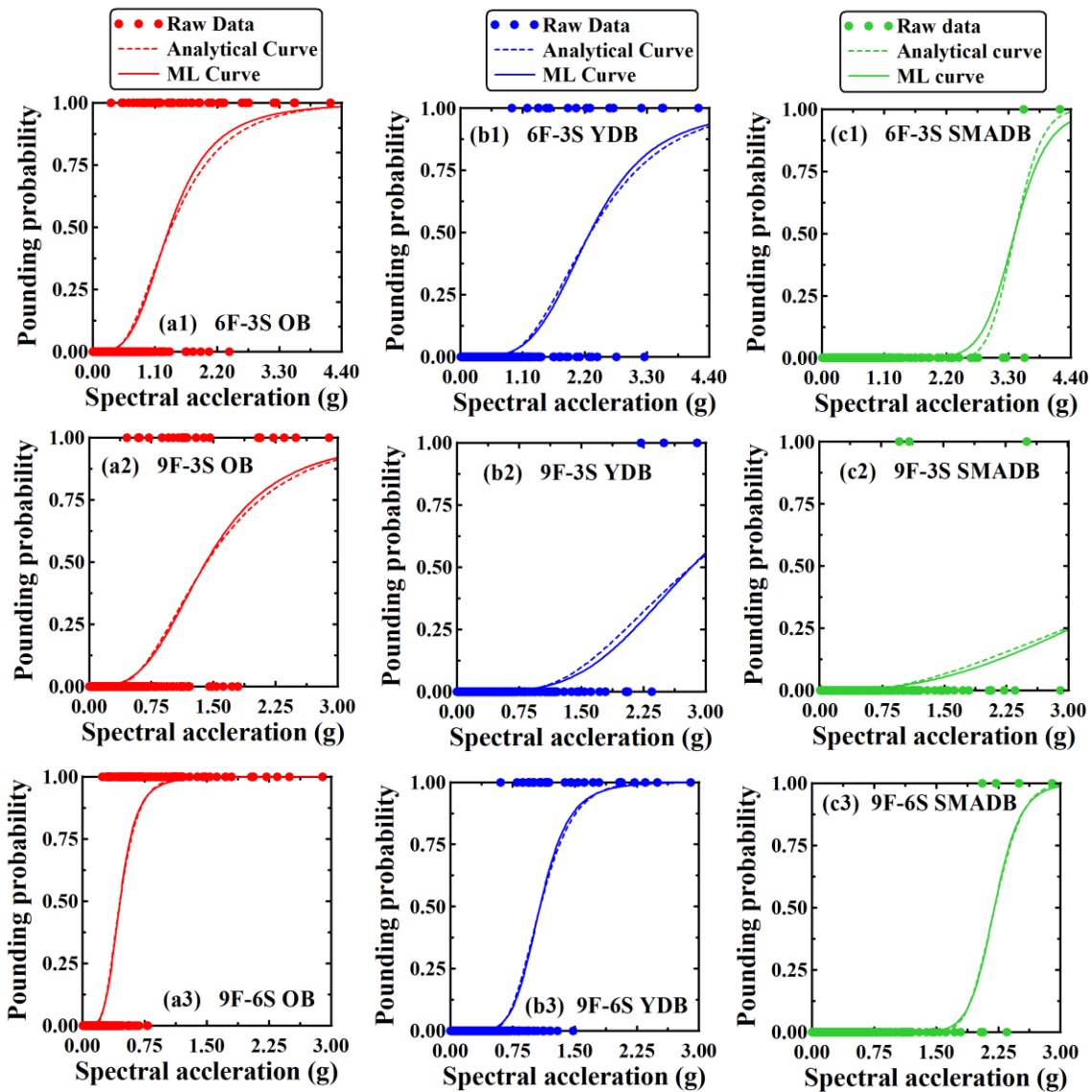


Fig. 11 Comparison of raw data, analytical and ML fragility curves of pounding for (a1)-(c1) 6F-3S (a2)-(c2) 9F-3S, and (a3)-(c3) 9F-6S buildings

Table 4: Logistic regression curves parameters for overall pounding fragility

Building combination	Slope (w)			Bias (θ)		
	OB	YDB	SMADB	OB	YDB	SMADB
6F-3S	3.52	4.08	11.52	-1.18	-3.38	-14.12
9F-3S	3.23	3.90	10.51	-1.11	-4.06	-13.88
9F-6S	4.54	6.22	14.06	-3.62	-4.88	-16.11

Similarly, Fig. 11 (a3) to (c3) compares the ML based fragility curves with the analytical fragility curves for 6F-3S building, without and with YD and SMAD. In this case, almost no difference is observed between ML based and analytical fragility curves. This proves the robust feature of ML based logistic regression method to predict the pounding vulnerability under seismic loading. Table 4 provides the logistic regression model parameters (slope and bias) for different combination of buildings, without and with YD and SMAD. As can be observed, for SMAD connected buildings, values of slope and bias parameters are much different than unconnected and YD connected buildings.

7. CONCLUSIONS

Present study describes the application of SMAD as a potential seismic retrofitting device for pounding vulnerability reduction of adjacent building structures and compare the results with the YD. To this end, optimally designed YD and SMAD are considered and used to connect 3, 6, and 9 story SMRF buildings with different combinations such as 6F-3S, 9F-3S, and 9F-6S. To assess the effectiveness of YD and SMAD, NLTHAs are conducted using 400 ground motions which are scaled to match a specific level of response spectra, as per ASCE 7-10 code. The result of 400 NLTHAs are used to predict pounding control efficiency of YD and SMAD and compared for a wide range of S_a . Severity of pounding is quantified based on three different damage states (such as 1/3 floor pounding, 2/3 floor pounding, and all floor pounding) to quantify the individual floor level pounding, and group together as overall pounding to quantify system level pounding. Study results indicate that, the SMAD significantly reduces the pounding induced damage (both individual floor level and overall), almost above 90% and 80% than the unconnected building and YD connected building, respectively. Subsequently, the pounding vulnerability (probability) has been predicted in terms of the S_a , through fragility analysis. As found from the overall and individual damage state fragility curves, SMAD significantly enhances the pounding resistance capacity and noticeably reduces the uncertainty in pounding prediction, when compare with the unconnected and YD connected building. In terms of the fragility curve parameters, compare to YD, SMAD increases the median value of S_a (i.e. the pounding resistance capacity) by 50 % to 100 %, and reduces the log standard deviation value of S_a (i.e. uncertainty in the prediction of the pounding probability) by 40 % to 50 %. In the end, as an alternative to the analytical fragility curve method, ML base logistic regression method is proposed to predict the pounding vulnerability. It has been found that, ML based fragility curve agrees very well with the analytical fragility curve and gives sufficient prediction of pounding probability. Thus, taken together all of the results, it can be stated that SMAD substantially reduces seismic pounding probability than the unconnected building and

YD connected building. ML based method predicts very well the pounding vulnerability similar as analytical fragility curve method.

ACKNOWLEDGEMENTS

Financial support provided by the Department of Science and Technology (DST) of the Government of India, through the Start-up Research Grant (SRG/2020/000892) by the Science and Engineering Research Board (SERB) is acknowledged.

REFERENCES

- Bhaskararao, A.V. and Jangid, R.S. (2006), "Harmonic response of adjacent structures connected with a friction damper." *J. Sound Vib.*, Vol. **292**(3-5), 710-725.
- Bhaskararao, A.V. and Jangid, R.S. (2006), "Seismic response of adjacent buildings connected with friction dampers." *Bull. Earthquake Eng.*, Vol. **4**, 43-64.
- DesRoches, R. and Smith, B. (2004), "Shape memory alloys in seismic resistant design and retrofit: a critical review of their potential and limitations." *J. Earthquake Eng.*, Vol. **8** (3), 415-429.
- Dolce, M., Cardone, D. and Marnetto, R. (2000), "Implementation and testing of passive control devices based on shape memory alloys." *Earthquake Eng. Struct. Dyn.*, Vol. **29**(7), 945-968.
- Domenico, D.D. and Gandelli, E. (2021), "Advanced modeling of SMA flag-shaped hysteresis for nonlinear time-history analysis in SAP2000." *J. Struct. Eng.*, Vol. **147**(11), 06021004.
- Ge, D.D., Zhu, H.P., Wang, D.S. and Huang, M.S. (2010), "Seismic response analysis of damper-connected adjacent structures with stochastic parameters." *J. Zhejiang Univ. Sci. A*, Vol. **11**(6), 402-414.
- Graesser, E.J. and Cozzarelli, F.A. (1991), "Shape-memory alloys as new materials for aseismic isolation." *J. Eng. Mech.*, Vol. **117**(11), 2590-2608.
- Gur, S., Mishra, S.K. and Roy, K. (2016), "Stochastic seismic response of building with super-elastic damper." *Mech. Syst. Signal Process.*, Vol. **72-73**, 642-659.
- Gur, S., Xie, Y. and DesRoches, R. (2019), "Seismic fragility analyses of steel building frames installed with superelastic shape memory alloy dampers: comparison with yielding dampers." *J. Intell. Mater. Syst. Struct.*, Vol. **30**(18-19), 2670–2687.
- Gur, S., Singh, P. and Roy, K. (2020), "Seismic response of adjacent building structure connected with superelastic damper: comparison with yield damper", *Proceedings of 11th International Conference on Structural Dynamics (EURODYN 2020)*, Greece.
- Gur, S., Roy, K. and Singh, P. (2022), "Seismic performance assessment of adjacent building structures connected with superelastic shape memory alloy damper and comparison with yield damper", *Struct. Control Health Monit.*, Vol. **29**(5), e2926.
- Han, Y.L., Li, Q.S., Li, A.Q., Leung, A.Y.T. and Lin, P.H. (2003), "Structural vibration control by shape memory alloy damper." *Earthquake Eng. Struct. Dyn.*, Vol. **32**(3), 483-494.
- Janke, L., Czaderski, C., Motavalli, M. and Ruth, J. (2005), "Applications of shape memory alloys in civil engineering structures – overview, limits and new ideas." *Mater. Struct.*, Vol. **38**, 578–592.

- Jameel, M., Islam, A.B.M., Hussain, R.R., Hasan, S.D., and Khaleel, M. (2013), "Non-linear FEM analysis of seismic induced pounding between neighbouring multi-storey structures." *Lat. Am. J. solids struct.*, Vol. **10**(5), 921-939.
- Kazemi, F., Mohebi, B., and Yakhchalian, M. (2020), "Predicting the seismic collapse capacity of adjacent structures prone to pounding." *Can. J. Civ. Eng.*, Vol. **47**(6), 663-677.
- Kazemi, F., Miari, M. and Jankowski, R. (2021), "Investigating the effects of structural pounding on the seismic performance of adjacent RC and steel MRFs." *Bull. Earthquake Eng.*, Vol. **19**(1), 317-343.
- Kazemi, F., Mohebi, B. and Jankowski, R. (2021), "Predicting the seismic collapse capacity of adjacent SMRFs retrofitted with fluid viscous dampers in pounding condition." *Mech. Syst. Signal Process.*, Vol. **161**, 107939.
- Kitayama, S. and Constantinou, M.C. (2016), "Probabilistic collapse resistance and residual drift assessment of buildings with fluidic self-centering systems." *Earthquake Eng. Struct. Dyn.*, Vol. **45**(12), 1935–1953.
- Matsagar, V.A. and Jangid, R.S. (2005), "Viscoelastic damper connected to adjacent structures involving seismic isolation." *J. Civ. Eng. Manage.*, Vol. **11**(4), 309-322.
- Matsagar, V.A. and Jangid, R.S. (2006), "Base-isolated building connected to adjacent building using viscous dampers." *Bull. N. Z. Soc. Earthq. Eng.*, Vol. **39**(1), 59-80.
- Ni, Y.Q., Ko, J.M. and Ying, Z.G. (2001), "Random seismic response analysis of adjacent buildings coupled with non-linear hysteretic dampers." *J. Sound Vib.*, Vol. **246**(3), 403-417.
- Ozbulut, O.E., Hurlebaus, S. and DesRoches, R. (2011), "Seismic response control using shape memory alloys: a review." *J. Intell. Mater. Syst. Struct.*, Vol. **22**(14), 1531-1549.
- Paola, M.D., Mendola, L.L. and Navarra, G. (2007), "Stochastic seismic analysis of structures with nonlinear viscous dampers." *J. Struct. Eng.*, Vol. **133**(10), 1475-1478.
- Paola, M.D. and Navarra, G. (2009), "Stochastic seismic analysis of MDOF structures with nonlinear viscous dampers." *Struct. Control Health Monit.*, Vol. **16**(3), 303-318.
- Patel, C.C. and Jangid, R.S. (2010), "Seismic response of adjacent structures connected with Maxwell dampers." *Asian J. Civ. Eng.*, Vol. **11**(5): 585–603.
- Patel, C.C. and Jangid, R.S. (2012), "Optimum parameter of viscous damper for damped adjacent coupled system." *J. Civ. Eng. and Sci.*, Vol. **1**(1), 22–30.
- Patel, C.C. (2022), "Seismic response control of parallel structures connected by passive shape memory alloy damper", *Proceedings of 12th Structural Engineering Convention (SEC 2022)*, Jaipur, India.
- Qian, H., Li, H., Song, G. and Guo, W. (2013), "Recentering shape memory alloy passive damper for structural vibration control." *Math. Probl. Eng.*, Vol. **2013**, 1–13.
- Qiu, C., Wang, H., Liu, J., Qi, J. and Wang, Y. (2020), "Experimental tests and finite element simulations of a new SMA-steel damper." *Smart Mater. Struct.*, Vol. **29**(3), 035016.
- Saadat, S., Salichs, J., Noori, M., Hou, Z., Davoodi, H., Bar-on, I., Suzuki, Y. and Masuda, A. (2002), "An overview of vibration and seismic applications of NiTi shape memory alloy." *Smart Mater. Struct.*, Vol. **11**(2), 218–229.
- Sama, K.J. and Gur, S. (2023), "Optimal design of SMA damper for vibration control of connected building under random seismic excitation", *Proceedings of 2nd International Conference on Construction Material and Structures (ICCMS 2022)*, Calicut, India.

*The 2023 World Congress on
Advances in Structural Engineering and Mechanics (ASEM23)
GECE, Seoul, Korea, August 16-18, 2023*

- Shinozuka, M., Feng, M.Q., Lee, J. and Naganuma, T. (2000), "Statistical analysis of fragility curves." *J. Eng. Mech.*, Vol. **126**(12), 1224-1231.
- Shinozuka, M., Feng, M.Q., Kim, H.K. and Kim, S.H. (2000), "Nonlinear static procedure for fragility curve development." *J. Eng. Mech.*, Vol. **126**(12), 1287-1295.
- Singh, P., Gur, S. and Roy, K. (2022), "Seismic Performance of Coupled Buildings Connected by Yield and SMA Dampers", *Proceedings of 12th Structural Engineering Convention (SEC 2022)*, Jaipur, India.
- Song, G., Ma, N. and Li, H.N. (2006), "Applications of shape memory alloys in civil structures." *Eng. Struct.*, Vol. **28**(9), 1266-1274.
- Takewaki, I. (2007), "Earthquake input energy to two buildings connected by viscous dampers." *J. Struct. Eng.*, Vol. **133**(5), 620-628.
- Yaghmaei-Sabegh, S. and Jalali-Milani, N. (2012), "Pounding force response spectrum for near-field and far-field earthquakes." *Sci. Iran.*, Vol. **19**(5), 1236-1250.
- Yan, X. and Nie, J. (2000), "Response of SMA superelastic systems under random excitation." *J. Sound Vib.*, Vol. **238**(5), 893-901.
- Zhang, W.S. and XU, Y.L. (2000), "Vibration analysis of two buildings linked by Maxwell model-defined fluid dampers." *J. Sound Vib.*, Vol. **233**(5), 775-796.
- Zhang, Y. and Zhu, S. (2007), "A shape memory alloy-based reusable hysteretic damper for seismic hazard mitigation." *Smart Mater. Struct.*, Vol. **16**(5), 1603-1613.
- Zhang, Y. and Zhu, S. (2008), "Seismic response control of building structures with superelastic shape memory alloy wire dampers." *J. Eng. Mech.*, Vol. **134**(3), 240-251.